Photovoltage detection of Damon-Eshbach and dipolar edge spin waves of nanomagnets with 2D electron gas system

N. K. A. Almulhem[1*], M. E. Stebliy[2], A. Nogaret[1], J. C. Portal[3], H. E. Beere[4], and D. A. Ritchie[4]

[1]*Department of Physics, University of Bath, Bath, BA2 7AY, UK*

[2]*Far Eastern Federal University, Laboratory of thin film technologies, Vladivostok 690950, Russia*

[3]*High Magnetic Field Laboratory, CNRS, 25 Avenue des Martyrs, 38042 Grenoble, France*

[4]*Cavendish Laboratory, JJ Thomson Avenue, Cambridge, CB3 0HE, UK*

[*]E-mail: N.K.A.Almulhem@bath.ac.uk

We report on a photovoltage technique which we use to probe spin excitations on submicron scales where surface effects play a dominant role. The localized spin waves modes were detected through the photovoltage induced in a two-dimensional electron gas system formed in a GaAs/AlGaAs heterojunction. The two-dimensional nature of the detector separates the effects of the in-plane and normal vector components of the magnetization. The high sensitivity of the technique arises from the low electron density and the high electron mobility of 2DEGs relative to metals. The large magnetoresistance further introduces nonlinearity in the Hall coefficient which magnifies the photovoltage. Localized modes of spin waves confined in the magnetostatic potential of the demagnetizing field are observed. We determine the dynamic properties of relevance to high-density information storage.

1. Introduction

Understanding the discrete modes of magnetic excitations of nanomagnets where surface effects play a dominant role, is essential for both fundamental science[1, 2] and applications[3, 4] to high-density information storage on hard disk drives which are accessed at increasingly high frequencies (GHz).[5] The collective dynamics of individual submicron magnets which are the most interesting is currently inaccessible by standard methods such as Brillouin Light Scattering (BLS)[6, 7] due to the need for a large volume of magnetic material to obtain an optical signal. This requires micromagnets to be arrayed instead of being probed individually.[8, 9]

BLS, one of the most significant techniques to investigate the dynamic properties of magnetic materials, gives information on energy losses incurred at momentum $\vec{\boldsymbol{q}} = \vec{\boldsymbol{k}} - \vec{\boldsymbol{k}}'$ where $\vec{\boldsymbol{k}}$ and $\vec{\boldsymbol{k}}'$ are the wavevectors of the incident and scattered photons. In this way, one can measure the energy-momentum $\boldsymbol{\omega}(\boldsymbol{q})$ dispersion curves of magnon.[10] The disadvantage of BLS is an optical technique that measures the energy of the momentum of spin wave in large scale samples ≥ 250 nm, greater than the wavelength of light. The present work has demonstrated a photovoltage spectroscopy technique which detects spin dynamics in submicron magnets.[7, 11, 12] Cobalt dots and wires generate inhomogeneous magnetic field near poles which confines localized spin wave modes.[6, 13] We show herein that the 2D electron gas (2DEG) is highly sensitive to the dynamics of ultra-small magnetic elements at its surface by rectifying high frequency oscillation of the magnetization.

Our sample consists of individual cobalt stripes 80 nm wide and 30 nm thick which were placed at the centre of a Hall bar made of a GaAs/AlGaAs heterojunction.[14-16] The results show (i) Damon–Eshbach modes which propagate along the edge parallel to the dc magnetic field at different frequencies and at low-temperatures.[10, 17-19] (ii) Strong bulk-edge mode coupling was observed as a bonding-antibonding gap at the resonance when the magnetization is perpendicular.[20] (iii) Comparison of experimental measurement and micromagnetic simulation were made using OOMMF.[21] Our photovoltage technique can pick up the resonance of localized magnetic moments through the eddy current they induce in the high mobility 2DEG. We varied parameters such as the field orientation and the geometry of nanomagnets. The photovoltage of the perpendicularly magnetized stripe is larger because of the greater modulation induced than in the parallel configuration.

2. Methods

2.1 Devices and photovoltage measurements

We first built a low-temperature microwave bench which applied a magnetic field $\boldsymbol{B_{dc}}$ to the sample using two NdFeB magnets. The magnetic field was varied at the site of the sample by symmetrically sliding the magnets away from the sample site by varying the distance from 11 mm to 50 mm. It follows that the magnetic field strength was varied from 0.606 T to 0.083 T. The sample was iradiated by a microstrip antenna placed in a slot directly above it, Fig. 1(a).[22, 23] Details of the slot and microstrip antenna are shown in Fig. 1(b). Our samples are hybrid devices consisting of a Hall bar topped with a Co bar magnet of sub-100nm cross section. Figure. 1(c) shows a higher resolution SEM of one of the devices which has a 80 nm wide, 30 nm high Co stripe in the active region of the Hall bar. [14, 16] The voltage probes were separated by 2-16 μm gaps. Our photovoltage was measured across 8 μm probes. Figure. 1(d) indicates the configuration of magnetic resonance in the hybrid devices**.** The two-dimensional electron gas had a micromagnetic element located at its centre. The GaAs/AlGaAs heterojunction hosting the 2DEG was 30 nm below the surface. The sensitivity of photovoltage measurements arises from the high electron mobility of our semiconductor heterojunction which is $\mu = 1.5 \times 10^6 cm^2.V^{-1}.S^{-1}$ and higher than that of bulk metals generating >100 times greater electromotive force.

In a low magnetic field experiment, the sample was cooled down to 77K by a cold finger polytetrafluoroethylene pot with a cooper base. We applied microwaves at frequency $\boldsymbol{\hbar\omega}$ through a planar microstrip antenna which transmits the radiation directly to the stripe magnet.[24] High magnetic field experiments were also conducted in which microwaves were guided via an overmoded waveguide to the sample space of a 17T superconducting magnet. The sample was maintained at 1.3K by a variable temperature insert. A range of backward wave oscillators was used to generate microwaves over frequencies $\boldsymbol{\omega/2\pi}$ = 30 GHz to 130 GHz. The magnetic field component of these microwaves $\boldsymbol{B_{ac}}$ drives spin resonance. The oscillations of the magnetization induce a Faraday electric field which drives a.c currents in the 2DEG. These currents result from oscillations of the magnetization which induce an alternative fringe field $\boldsymbol{B_m}$ at the site of the 2DEG. $\boldsymbol{B_m}$ deflects eddy currents via the Hall effect in the direction perpendicular to the bar magnet. The rectified Hall voltage generated across the bar magnet is:

$$PhV = \mu\, \mu_0^2\, A\, \langle M_z \dot{M}_x - M_x \dot{M}_z \rangle \qquad (1)$$

where $\boldsymbol{\mu}$ is the electron mobility in the 2DEG, $\boldsymbol{\mu_0}$ is the magnetic permeability, $\boldsymbol{A}$ is the effective area which is approximately the square of the decay length of the stray magnetic field, and $\boldsymbol{M_x}$ and $\boldsymbol{M_z}$ the magnetization component, Fig. 1(d). We consider the influence of the magnetic field $\boldsymbol{B_{dc}}$ applied either parallel or perpendicular to the magnetic stripe. The Co magnetization precesses at a frequency $\boldsymbol{\omega_0}$, which is proportional to the magnitude of the static magnetic field, $\boldsymbol{B_{dc}}$. At resonance $\boldsymbol{\omega = \omega_0}$, the magnetization oscillates back and forth parallel and antiparallel to $\boldsymbol{B_{dc}}$ giving peaks in photovoltage according to Eq.1.

2.2 micromagnetic simulations

We used the Object Oriented Micromagnetic Framework (OOMMF) simulation code to calibrate the collective oscillations of magnetic dipoles under the ac wave driving force and the dc external magnetic field.[25] One of the benefits of OOMMF is the ability to calculate the dephasing $\boldsymbol{\varphi}$ of the magnetization relative to the ac magnetic field. Then, using the phase difference $\boldsymbol{\varphi}$ to calculate the real and imaginary parts of the magnetic susceptibility as below [26, 27]:

$$\chi = \frac{M}{H} = \frac{M_0}{H_0} cos\varphi + \frac{M_0}{H_0} sin\varphi \frac{cos\omega t}{sin\omega t} \quad (2)$$

$$\chi' = \frac{M_0}{H_0} cos\varphi \quad (3)$$

$$\chi'' = \frac{M_0}{H_0} sin\varphi \quad (4)$$

$$\chi = \chi' + i\chi'' \quad (5)$$

Where H(t) is the periodic magnetic field, and M(t) is the periodic magnetic response, with microwave angular frequency $\boldsymbol{\omega}$. $\boldsymbol{\chi'}$ is a real susceptibility part which gives the speed of propagation of electromagnetic wave travel in the magnet. $\boldsymbol{\chi''}$is the imaginary susceptibility which corresponds to the absorption of microwave energy. The absorption $\boldsymbol{\chi''}$ has a Lorentzian frequency spectrum whose width increases with losses. Figures 2(a) and 3(a) show the magnetic response of the Co stripe under the action of the alternating field $\boldsymbol{B_{ac}}$ and the constant field $\boldsymbol{B_{dc}}$ in stripe geometry: 2000 nm × 220 nm × 40 nm; with mesh size 5 nm × 5 nm × 40 nm calculated using OOMMF simulation. The saturation magnetization of Co is $\mu_0 M_s$=1.77 T, the exchange interaction constant A = 30×10^{-12} J/m; K_1 = 0 J/m^3(since it is polycrystalline); the damping parameter is α = 0.05.[28, 29] Applying a small alternating field $\boldsymbol{B_{ac}}$ changes the magnetization over time for each cell and allows us to calculate the degree of magnetization of a sample and power which is absorbed.[30] $\boldsymbol{B_{dc}}$ was varied in the range [+5.0; -5.0] T with step of 0.005 T. After each increase in $\boldsymbol{B_{dc}}$ the system relaxed for 0.2 ns over 20

periods of the alternating field $B_{ac} = B_0 \sin(\omega t)$. The simulation was carried out for three frequencies: 55, 75, and 95 GHz. During excitation, the time dependence of the magnetization components was recorded with a time step of 1ps.

We defined the dynamical characteristic of nanostructure by using Fast Fourier Transformation to transfer magnetization as a function of time M(t) to magnetization as a function of frequency M(ω) to obtain the imaginary susceptibility $\boldsymbol{\chi''}$ as a function of magnetic field, Eq. (4). The imaginary susceptibility describes the phase shift of the magnetization and the microwave field.

From Eq. (2), $\chi'' = \frac{\boldsymbol{M_\perp}}{\boldsymbol{H}}$, $\boldsymbol{M_\perp}$ is always dissipative. The power absorbed per unit volume is [30-32]:

$$P = \frac{1}{2}\,\omega\,\boldsymbol{\chi''}\boldsymbol{H^2} \qquad (6)$$

Spatial map of the imaginary susceptibility shows the power absorbed over the sample at resonance.

3. Results and discussion

3.1 Results

3.1.1 B parallel to the long axis of Co stripe

In an infinite film, magnetic resonance is underpinned by a backward volume wave mode. In a stripe, at certain frequencies, and when $\boldsymbol{B_{dc}}$ is parallel to the long axis of Co stripe, the magnetostatic boundary conditions force spin wave modes to the surface of magnets. The stripe will then exhibit a backward volume mode modulated by Damon-Eshbach modes which propagate along the edges parallel to $\boldsymbol{B_{dc}}$. These resonant peaks are indicated by arrows labelled 1, 2, and 3 in Figs. 2(a) and (b). The OOMMF calculation of imaginary susceptibility depending on the frequency identifies peaks are corresponding to the positions of B_1=1.4 T at 55 GHz, B_2=1.98 T at 75 GHz, and B_3=2.34 T at 95 GHz, Fig. 2(a). In contrast, the locations of ferromagnetic resonance in the experimental photovoltage are B_1=1.33 T at 55 GHz, B_2=1.94 T at 75 GHz, and B_3=2.6 T at 95 GHz (Fig. 2(b)). We used the magnetic resonance equation $B = \frac{\hbar\omega}{g\mu_B}$ to calculate the position of peaks at each frequency, where $\boldsymbol{\mu_B}$ is the Bohr magneton and $\boldsymbol{g}$ is the $\boldsymbol{g}$-factor. The series of resonances calculated with OOMMF $\boldsymbol{\chi''}$ matches the magnetic fields corresponding the peaks position observed in the photovoltage spectroscopy. Both the amplitude of resonant peaks in micromagnetic simulation and in the photovoltage spectroscopy decreases with increasing frequency. This is because, although the microwave power $\boldsymbol{P}$ remained constant, $P = n \times \hbar\omega$, the increase in photon energy $\boldsymbol{\hbar\omega}$

caused the number of photons $\boldsymbol{n}$ to decrease. The amplitude of resonance is proportional to the number of photon which is absorbed. This is why the amplitude of resonant peaks decreases with increasing frequency.

3.2.1 Bonding-antibonding dipolar edge spin wave

The formation of confined spin waves relies both on quantum mechanical and classical principles. Exchange interaction aligns the spins of itinerant electrons. The magnetostatic potential of the demagnetizing field creates the boundary conditions which generate a discrete spectrum of spin wave frequencies. The confinement of spin waves produces discrete energy levels similar to those of electrons confined in a magnetic well when the $\boldsymbol{B_{dc}}$ perpendicular to the long axis of the stripe. The first energy level is corresponding to the discrete $\boldsymbol{n}$=1 is above the bottom of the well, second energy spacing when the $\boldsymbol{n}$=2 becomes larger than the first level. Subsequently, the energy minimization requires the largest wavelength, the total energy of the particle by the expression is:

$$E_n = \frac{n^2 h^2}{8mL^2} \tag{7}$$

The confinement of spin waves in bar magnets is produced by a strongly inhomogeneous static internal magnetic field. This inhomogeneity causes the creation of so-called spin-wave wells**.** The dispersion on the relation of a spin wave is given by Eq. (8) with frequency dependent on wavevector $\boldsymbol{q}$, the internal field $\boldsymbol{H}$, and stray magnetic field M(z). The variation of $\boldsymbol{M}$ compensates the variation of $\boldsymbol{q}$. Also, when $\boldsymbol{\omega_H}$ is bigger than $\boldsymbol{\omega}$, $\boldsymbol{q}$ is real at the centre of the stripe, but $\boldsymbol{q}$ becomes evanescent as the spin wave dispersion relation can be only fulfilled with an imaginary $\boldsymbol{q}$. The dispersion low for dipolar-exchange spin waves, having a wavevector parallel to the magnetic field in an infinite film is given by [6, 10, 33]:

$$\left(\frac{\omega}{\omega_M}\right)^2 = \left(\frac{\omega_H}{\omega_M} + \alpha q^2\right)\left[\frac{\omega_H}{\omega_M} + \alpha q^2 + 1 - \frac{1-exp(-qh)}{qh}\right] \tag{8}$$

From Eq. (8) there is a proportionality between $\boldsymbol{\omega}$ and $\boldsymbol{q}$ where $q_n = \frac{2\pi n}{L}$, $\boldsymbol{q}$ is continuous. The phenomena of the spin wave in the quantum well can be explained by the series of small resonances giving localized edge spin wave when $\boldsymbol{B_{dc}^{\perp}}$ to the stripe, Fig. 3(b). We study a bulk-edge mode when applying the field perpendicular to long edge of the stripe. The spin waves confined by the opposite edges overlap to produce one state localized in the centre of the stripe and another state which gives spin waves localized at the site of the two magnetic

wells at the edges.[34, 35] The former state occur at lower magnetic field and is the bonding state whereas the other is the antibonding state. These states are indicated by arrows 1 and 2 respectively in Figs. 3(a) and 4(b). We can compare the position of resonances in the micromagnetic simulation χ'' which are placed at B_1=1.6 T, B_2=2.2 T in 55 GHz while occurring at B_1=1.95 T and B_2=2.3 T in the photovoltage resonance. Figure 3(b) shows a series of small resonances (1, 2, … 5) associated with a quantized dipolar edge spin wave modes which include peaks 1 and 2. Comparing the amplitude of imaginary susceptibility peaks at $\boldsymbol{B}_{\boldsymbol{dc}}^{\parallel}$ and $\boldsymbol{B}_{\boldsymbol{dc}}^{\perp}$ with photovoltage resonance allows us to index the experimental peak. Peaks 1 and 2 in Fig. 3(a) are matches position of peaks 1 and 2 in Fig. 3(b). The good agreement between the experimental and predicted position of resonances which indicates the formation of bonding-antibonding pairs of edge spin waves.

3.2 Discussion

The results in a parallel magnetic field was more difficult to relate to the spatial distribution of the susceptibility because of the small values of the amplitude of ferromagnetic resonance, and the strong edge localization. The perpendicular field orientation was easier to interpret because the magnetostatic potential formed which provided a confining potential for spin waves. Figure. 2(a) has small additional peaks at vanishing magnetic field. There are no peaks corresponding to the zero frequency in the simulation. Furthermore, the simulation differs from the experimental structure below the main resonance in Figs. 2 and 3. On the other hand, the amplitude of experimental ferromagnetic resonance decays faster in $\boldsymbol{B}_{\boldsymbol{dc}}^{\parallel}$than $\boldsymbol{B}_{\boldsymbol{dc}}^{\perp}$ as microwave frequency increases. In the perpendicular configuration, the susceptibility resonances in $\boldsymbol{B}_{\boldsymbol{dc}}^{\perp}$ are better defined than in the $\boldsymbol{B}_{\boldsymbol{dc}}^{\parallel}$ to the stripe. The photovoltage is larger when $\boldsymbol{B}_{\boldsymbol{dc}}^{\perp}$ in Fig. 3 than when the $\boldsymbol{B}_{\boldsymbol{dc}}^{\parallel}$ in Fig. 2. The localization of edge spin waves in $\boldsymbol{B}_{\boldsymbol{dc}}^{\perp}$ is stronger than in the Damon-Eshbach scenario when $\boldsymbol{B}_{\boldsymbol{dc}}^{\perp}$.

4. Conclusions

Through the results presented here, we have summarized photovoltage spectroscopy to be a powerful technique for probing a magnetic excitation of scale lower than 100 nm which is inaccessible by Brillouin Light scattering. We also describe the discrete structure of spin wave resonance as a function of magnetic field orientation which is parallel or perpendicular to the magnetic stripe and the geometry of nanomagnets. The sensitivity of this technique has revealed the theoretically predicted fine structure of confined spin waves and is likely to

provide further insights into the magnetic properties of individual nanomagnets. There are additional experimental resonances which are not explained by the theory, and which most likely arise from 3D volume spin waves not accounted for by OOMMF magnetic simulation.

Acknowledgments

This work was supported by FP7-2012-IRSES under grant number 318973. Najla Almulhem acknowledges support from the Ministry of Education in Saudi Arabia, and Saudi Arabian Cultural Bureau in London for making it possible to undertake this work.

Appendix

References

1) A. Fernandez-Pacheco, R. Streubel, O. Fruchart, R. Hertel, P. Fischer and R. P. Cowburn, Nat Commun **8**, 15756 (2017).
2) T. Shinjo, T. Okuno, R. Hassdorf, K. Shigeto and T. Ono, Science **289** (5481), 930-932 (2000).
3) J.-G. Zhu, Y. Zheng and G. A. Prinz, Journal of Applied Physics **87** (9), 6668-6673 (2000).
4) M. Miller, G. Prinz, S.-F. Cheng and S. Bounnak, Applied Physics Letters **81** (12), 2211-2213 (2002).
5) A. L. Barra, D. Gatteschi and R. Sessoli, Physical Review B **56** (13), 8192 (1997).
6) C. W. Sandweg, M. B. Jungfleisch, V. I. Vasyuchka, A. A. Serga, P. Clausen, H. Schultheiss, B. Hillebrands, A. Kreisel and P. Kopietz, Rev Sci Instrum **81** (7), 073902 (2010).
7) M. Harder, Y. Gui and C.-M. Hu, Physics Reports **661**, 1-59 (2016).
8) G. Gubbiotti, S. Tacchi, G. Carlotti, N. Singh, S. Goolaup, A. Adeyeye and M. Kostylev, Applied Physics Letters **90** (9), 092503 (2007).
9) M. Kostylev, G. Gubbiotti, J.-G. Hu, G. Carlotti, T. Ono and R. Stamps, Physical Review B **76** (5), 054422 (2007).
10) C. Bayer, Jorzick, J., Demokritov, S.O., Slavin, A.N., Guslienko, K.Y., Berkov, D.V., Gorn, N.L., Kostylev, M.P. and Hillebrands, B., in *Spin dynamics in confined magnetic structures III* (Springer, 2006), pp. 57--103.
11) M. Harder, Z. X. Cao, Y. S. Gui, X. L. Fan and C. M. Hu, Physical Review B **84** (5) (2011).
12) Y. Tserkovnyak, Brataas, A., Bauer, G.E. and Halperin, B.I., Reviews of Modern Physics **77** (4), 1375 (2005).
13) L. C. Branquinho, M. S. Carriao, A. S. Costa, N. Zufelato, M. H. Sousa, R. Miotto, R. Ivkov and A. F. Bakuzis, Sci Rep **3**, 2887 (2013).
14) A. Nogaret, J Phys Condens Matter **22** (25), 253201 (2010).
15) D. Uzur, A. Nogaret, H. E. Beere, D. A. Ritchie, C. H. Marrows and B. J. Hickey, Physical Review B **69** (24) (2004).
16) A. Nogaret, D. N. Lawton, D. K. Maude, J. C. Portal and M. Henini, Physical Review B **67** (16), 165317 (2003).
17) D. N. Lawton, A. Nogaret, S. J. Bending, D. K. Maude, J. C. Portal and M. Henini, Physical Review B **64** (3), 033312 (2001).
18) J. P. Park, P. Eames, D. M. Engebretson, J. Berezovsky and P. A. Crowell, Phys Rev Lett

89 (27), 277201 (2002).

19) R. W. a. E. Damon, J.R., Journal of Physics and Chemistry of Solids **19** (3-4), 308--320 (1961).
20) P. Saraiva, A. Nogaret, J. C. Portal, H. E. Beere and D. A. Ritchie, Physical Review B **82** (22), 224417 (2010).
21) Y. S. Gui, S. Holland, N. Mecking and C. M. Hu, Phys Rev Lett **95** (5), 056807 (2005).
22) V. Bernard, & Iloh, J. P. I., International Journal of Emerging Technology and Advanced Engineering **3** (11) (2013).
23) J. R. James, P. S. Hall and C. Wood, *Microstrip antenna: Theory and design*. (McGraw-Hill, Inc., 1981).
24) I. Singh, & Tripathi, V. S., Int. J. Comp. Tech. Appl **2** (5), 1595--1599 (2011).
25) U. G. Ahmad, Shukur, S. and Ridwan, A.I., International Journal of Engineering Science **3811** (2016).
26) V. Donchev, T. Ivanov, K. Germanova and K. Kirilov, Spectroscopy **8** (2010).
27) N. Vukadinovic and F. Boust, Physical Review B **75** (1), 014420 (2007).
28) M. E. Stebliy, S. Jain, A. G. Kolesnikov, A. V. Ognev, A. S. Samardak, A. V. Davydenko, E. V. Sukovatitcina, L. A. Chebotkevich, J. Ding, J. Pearson, V. Khovaylo and V. Novosad, Sci Rep **7** (1), 1127 (2017).
29) S. Michea, Briones, J., Palma, J.L., Lavín, R., Escrig, J., Rodríguez-Suárez, R. and Denardin, J.C., arXiv preprint arXiv:1401.6064 (2014).
30) A. Kaya and J. A. Bain, Journal of Applied Physics **99** (8), 08B708 (2006).
31) R. M. White, R. M. White and B. Bayne, *Quantum theory of magnetism*. (Springer, 1983).
32) E. Levin, V. Pecharsky and K. Gschneidner Jr, Journal of Applied Physics **90** (12), 6255-6262 (2001).
33) C. Berger, Song, Z., Li, X., Wu, X., Brown, N., Naud, C., Mayou, D., Li, T., Hass, J., Marchenkov, A.N. and Conrad, E.H., Science **312** (5777), 1191--1196 (2006).
34) J. A. C. Bland, Hirohata, A., Xu, Y.B., Guertler, C.M. and Holmes, S.N., IEEE transactions on magnetics **36** (5), 2827--2832 (2000).
35) A. Nogaret, Stebliy, M., Portal, J.C., Samardak, A., Ognev, A., Beere, H. and Ritchie, D., Solid State Phenomena **215**, 400--406 (2014).

Figure Captions

Fig. 1. (a) The side view of the rig setup consisting of two permanent magnets, the sample is placed at the centre of the bench. Above the sample is a microwave antenna holder. (b) The top view shows a Microstrip antenna that emits microwaves towards the sample. (c) The top panel is a higher resolution SEM of a Hall bar showing all 14 voltage and current probes with their Ohmic contact pads. The current probes are contacts 1 and 8 and the rest of the contacts are voltage probes. The bottom panel shows a Cobalt stripe in the middle of the Hall bar 30 nm high, and 80 nm width. (d) Schematics of the micro-magnetic stripe magnetized in the plane of the 2DEG by $\boldsymbol{B_{dc}}$ and driven to resonance by $\boldsymbol{B_{ac}}$.

Fig. 2. a) Experimental dependence of the photovoltage with $B_{\parallel}$ to the stripes. The amplitude of the resonance decreases with increasing frequency. (b) Calculation of the imaginary susceptibility in parallel magnetic field at different frequencies.

Fig. 3. a) Experimental dependence of the photovoltage with $B_{\perp}$ to the stripes, and there are some additional peaks. (b) Calculation of the imaginary susceptibility showing a bonding and antibonding peaks 1 and 2.

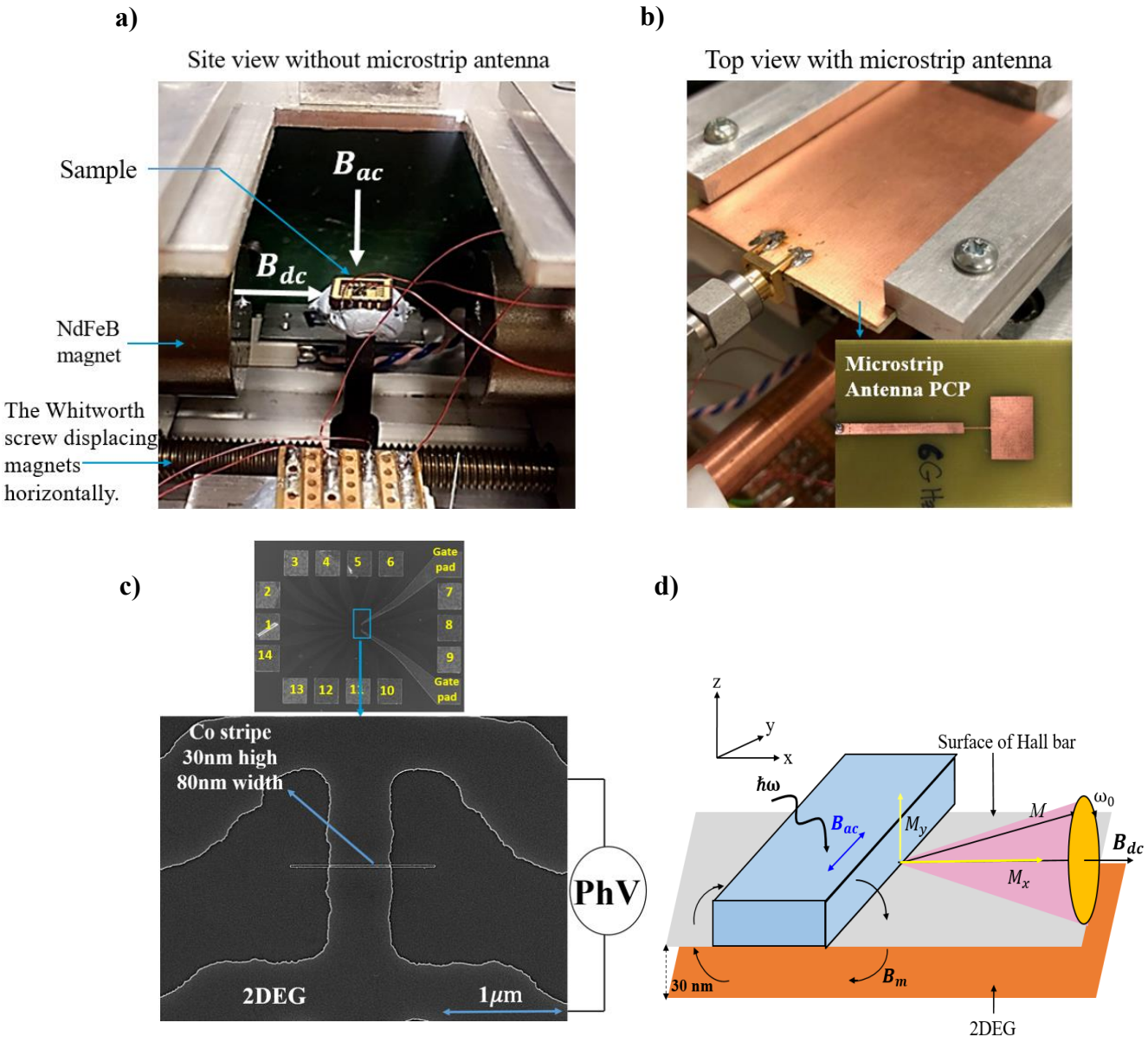

Fig.1. (Color Online)

Color print

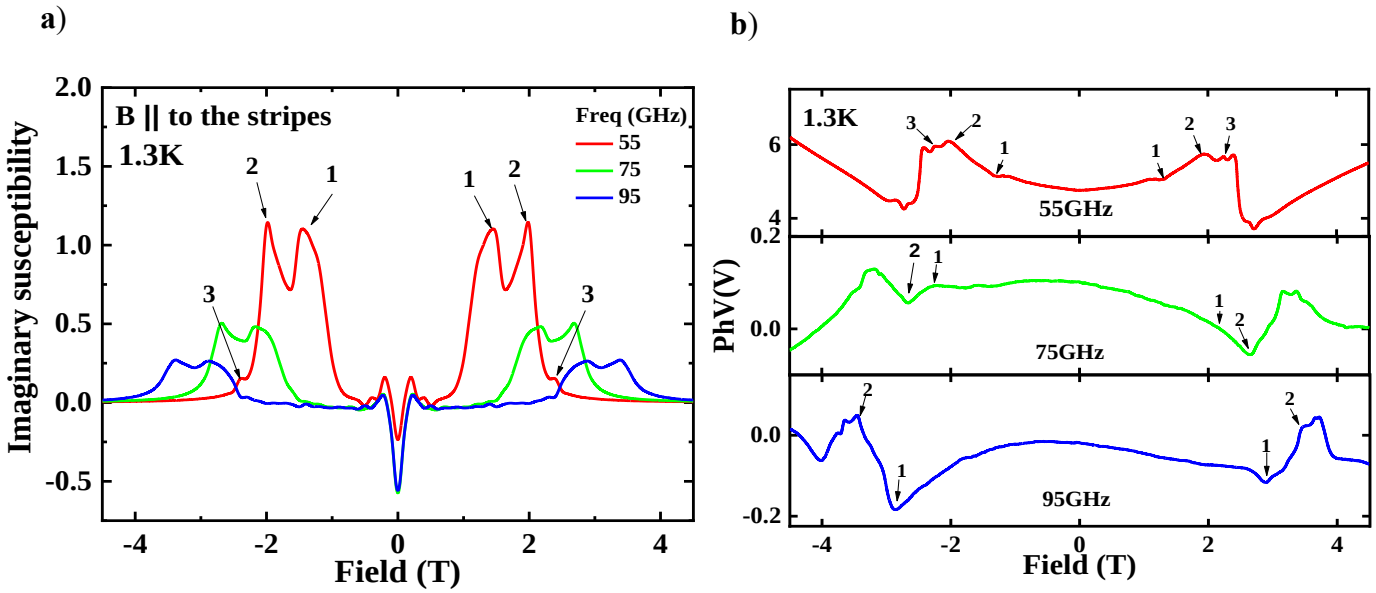

Fig.2. (Color Online)

Color print

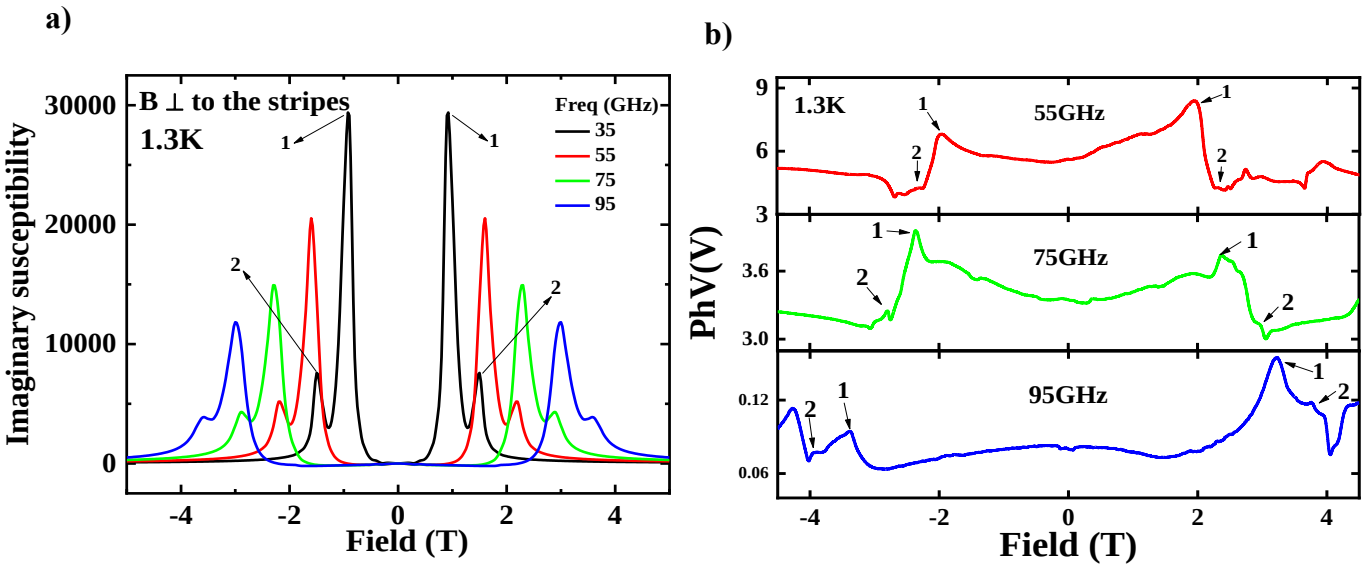

Fig. 3. (Color online)

Color print